



Fluorescence imaging through dynamic scattering media with speckle-encoded ultrasound-modulated light correlation

Haowen Ruan^{1,2}✉, Yan Liu^{1,2}✉, Jian Xu¹, Yujia Huang¹ and Changhui Yang¹✉

Fluorescence imaging is indispensable to biomedical research, and yet it remains challenging to image through dynamic scattering samples. Techniques that combine ultrasound and light as exemplified by ultrasound-assisted wavefront shaping have enabled fluorescence imaging through scattering media. However, the translation of these techniques into *in vivo* applications has been hindered by the lack of high-speed solutions to counter the fast speckle decorrelation of dynamic tissue. Here, we report an ultrasound-enabled optical imaging method that instead leverages the dynamic nature to perform imaging. The method utilizes the correlation between the dynamic speckle-encoded fluorescence and ultrasound-modulated light signal that originate from the same location within a sample. We image fluorescent targets with an improved resolution of $\leq 75\ \mu\text{m}$ (versus a resolution of 1.3 mm with direct optical imaging) within a scattering medium with 17 ms decorrelation time. This new imaging modality paves the way for fluorescence imaging in highly scattering tissue *in vivo*.

Optical imaging is indispensable to many research areas because it benefits from a wide range of light–matter interaction mechanisms and a host of endogenous and exogenous contrast agents. However, optical imaging through opaque scattering media, such as biological tissue, has long been a highly challenging problem^{1–6}. The randomization of the optical wavefront due to scattering is one aspect of the challenge—it scrambles the optical information in space. Although methods such as wavefront shaping have begun to address this challenge^{7–13}, the dynamic nature of some of these scattering media, which living tissue is a prominent example, adds another dimension to the challenge^{14–16}. The dynamic nature leads to rapid decorrelation of optical information in time and necessitates the use of fast techniques to capture optical information before it is scrambled^{16–29}.

In comparison, ultrasound scatters much less than light in soft tissue and is therefore extensively used to perform imaging inside tissue. However, ultrasound imaging does not have as wide range of contrast mechanisms and contrast agents and therefore reveals less functional information. As such, methods that can synergistically combine the advantages of sound and light are highly desirable. One example is photoacoustic imaging³⁰, which relies on the thermal expansion of optical absorptive objects to generate ultrasound signals. An interesting development in photoacoustics is the use of the dynamic property of speckles or samples to improve spatial resolution^{31–33}—a development that shares some roots with the method we are reporting here. While photoacoustics provides good absorption contrast in images, it is not well suited for obtaining fluorescence contrast—probably the most important optical contrast in biomedical research³⁴.

There have been several notable attempts at introducing fluorescence imaging capability into ultrasound-mediated optical imaging. These approaches include using ultrasound to directly modulate fluorescence^{35,36} and using engineered fluorescence microbubbles³⁷, liposomes³⁸ or thermosensitive polymers³⁹ as contrast agents to enhance the ultrasound-modulated fluorescence signal. However,

direct fluorescence modulation has an extremely low modulation efficiency, and the introduction of special exogenous agents restricts the application range of such techniques. On a different front, ultrasound-assisted optical wavefront shaping methods, as exemplified by time-reversed ultrasonically encoded (TRUE) optical focusing^{40–42}, employ focused ultrasound as a guidestar⁴³ to generate an optical focus inside a scattering medium. The optical focus can be used to perform fluorescence excitation and raster-scanning imaging. However, like other wavefront shaping methods, this approach is currently confounded by the rapid optical speckle decorrelation in living animals and the lack of high-speed phase conjugation solutions^{15,16}. The rapid optical speckle decorrelation in living animals depends on the tissue type as well as on the probing depth^{15,16,44}, and as it is an intrinsic property of living tissue, leveraging it for use rather than treating it as a challenge may be more fruitful.

Here, we report an ultrasound-enabled fluorescence imaging method that works in highly dynamic scattering media. In this method, the ever-changing nature of speckle patterns inside a time-varying scattering sample is not an impediment, but is instead a key enabling mechanism. In our case, the ultrasound-modulated light signal associated with an ultrasound focus in a dynamic scattering medium directly correlates with the fluctuating speckle intensity at that location. Likewise, the fluorescence signal from the same location is correlated with the fluctuating speckle intensity. As such, by measuring and correlating the ultrasound-modulated light signal and the fluorescence signal from the sample, we can isolate the fluorescence signal emanating from the target location defined by the ultrasound focus. By scanning the ultrasound focus and repeating the above process, we can obtain an image of the fluorescent objects within the scattering medium. We termed the method FLuorescence and Ultrasound-modulated light Correlation or FLUX (X for correlation) for short.

FLUX enables imaging of fluorescent objects inside a scattering medium exhibiting fast speckle decorrelation. A key challenge with wavefront shaping methods such as TRUE focusing is that the

¹Department of Electrical Engineering, California Institute of Technology, Pasadena, CA, USA. ²These authors contributed equally: Haowen Ruan, Yan Liu. ✉e-mail: hruan@caltech.edu; yanliu@caltech.edu; chyang@caltech.edu

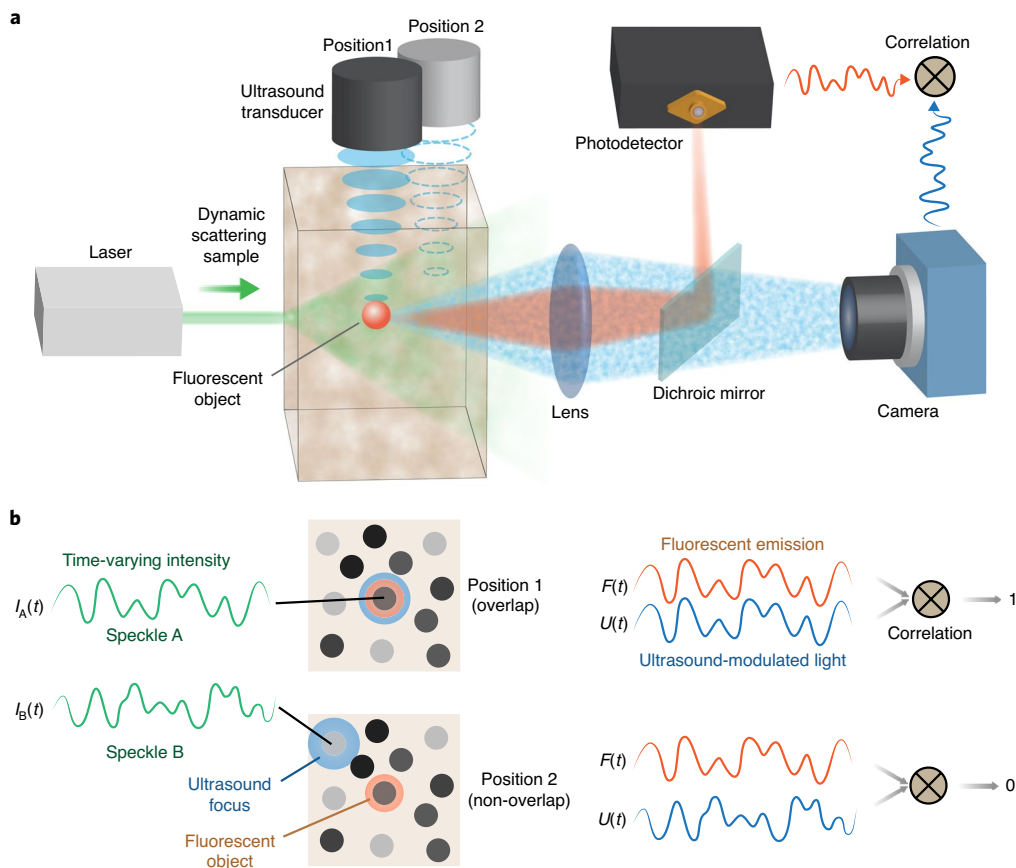


Fig. 1 | Principle of FLUX. **a**, Simplified set-up. A laser beam excites a fluorescent object inside a dynamic scattering sample. Meanwhile, a focused ultrasound beam modulates the photons passing through the ultrasound focus. The fluorescent light and ultrasound-modulated light are separated by a dichroic mirror and simultaneously measured by a photodetector and a camera, respectively. At position 1, the ultrasound focus overlaps with the fluorescent object; at position 2, the ultrasound focus is away from the object. **b**, Illustration of signals. A fluorescent object located at speckle A emits a fluctuating fluorescence signal in sync with the time-varying speckle intensity. Likewise, an ultrasound focus located at speckle A generates a fluctuating ultrasound-modulated light signal in sync with the speckle intensity. Hence, the correlation of the fluorescence and ultrasound-modulated light signals would be high (upper panel). If the ultrasound focus is instead located at a different speckle (speckle B), the correlation of the two signals would be low (lower panel).

process of wavefront shaping needs to be completed within a speckle decorrelation time. FLUX does not involve such complex, active wavefront manipulation and instead simply passively measures the time traces of the acousto-optical signal and the fluorescence signal.

Results

Principles. The principle of FLUX is illustrated in Fig. 1. A simplified experimental set-up is shown in Fig. 1a. A coherent laser beam is used to excite a fluorescent object inside a dynamic scattering sample. As the light beam enters the sample, speckles develop due to interference of multiply scattered light. Within the sample, the fully developed speckles are highly independent of each other and randomly distributed in space. In time, the speckle pattern fluctuates due to the dynamic property of the sample and becomes uncorrelated after a decorrelation time interval. Therefore, the speckle intensity varies in both space and time, which makes it difficult for conventional imaging methods to probe the optical information inside the scattering medium. Here, we turn this problem into an enabling mechanism to uniquely encode the optical information inside the scattering medium. A fluorescent object sees its local speckle pattern as a time-varying excitation source, and it emits a time-varying fluorescence signal that mirrors the speckle intensity changes. Because the time-varying speckle intensity is independent at each spatial speckle, the locations of the fluorescent targets are uniquely encoded by this time-varying excitation. Outside the sample,

a photodetector collects the dynamic fluorescence signal $F(t)$, which is the aggregate of the time-varying fluorescence emissions from all the fluorophores within the sample.

We additionally transmit pulsed ultrasound through the sample to create an ultrasound focus at a target location. Light that travels through the ultrasound focus will have its frequency shifted by the ultrasound (that is, the acousto-optic effect^{45–47}), and we measure the amount of frequency-shifted photons outside the sample (see Methods for details on the measurement of the ultrasound-modulated light). The ultrasound-modulated light signal $U(t)$ would be directly proportional to the time-varying speckle intensity at the ultrasound focus position.

For simplicity, we assume that the ultrasound focus and the fluorescence object are of the same size. When the ultrasound focus overlaps with the fluorescent object (Fig. 1b, upper panel), they are illuminated by the same time-varying speckles. In this case, we can expect the fluorescence signal and ultrasound-modulated light signal to be highly correlated. This correlation should be low when the ultrasound focus and the fluorescent object are located on different illumination speckle grains (Fig. 1b lower panel). As such, by raster scanning the ultrasound focus and measuring the correlation at each ultrasound focus location, an image of the fluorescent object can be obtained.

Importantly, the speckle decorrelation affects only the measurement of the ultrasound-modulated light signal and fluorescence

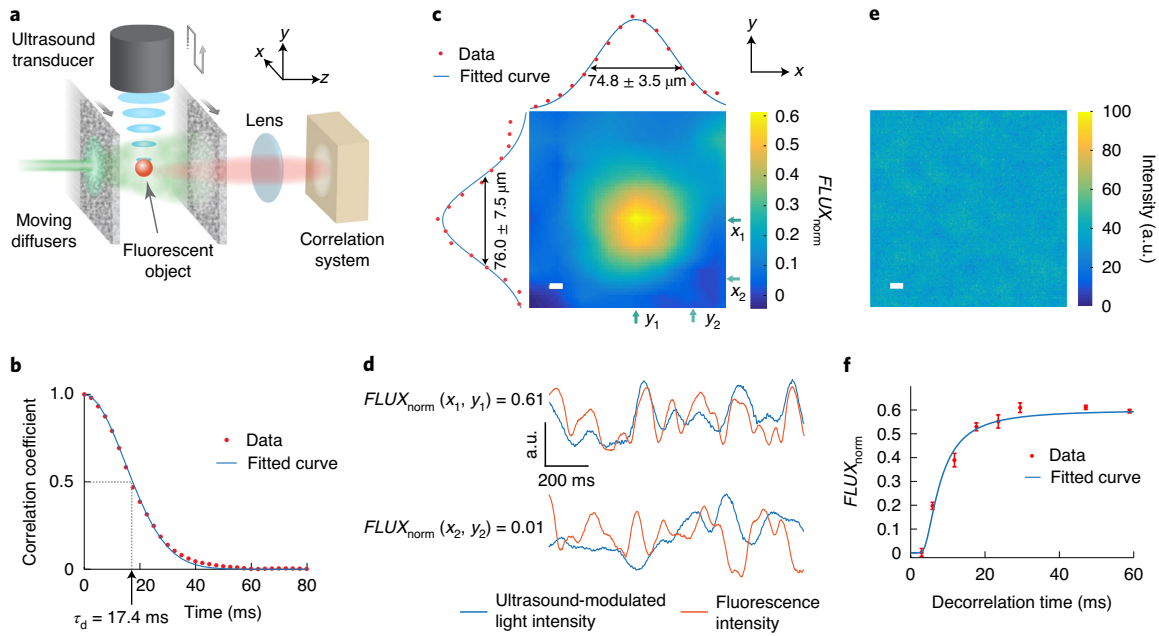


Fig. 2 | Imaging a fluorescent target inside a dynamic scattering sample and characterizing the system performance. **a**, Simplified set-up. **b**, Speckle decorrelation curve calculated from the correlation of the time-lapse speckle patterns recorded on the camera plane when the diffusers were moving. A decorrelation time of 17.4 ms was determined. **c**, Image of the fluorescent particle obtained by plotting $FLUX_{norm}$ as a function of the ultrasound focus position. A Gaussian model was used to fit the one-dimensional data across the peak of the image along the x and y directions, respectively. **d**, Sections of the exemplary signal traces obtained at the (x_1, y_1) and (x_2, y_2) locations denoted in **c**. **e**, Direct wide-field image of the fluorescent particle in the presence of the diffusers. The target cannot be discerned by a conventional imaging system due to scattering. **f**, $FLUX_{norm}$ as a function of decorrelation time. The error bars show the standard deviation of four measurements. Scale bars, 10 μm .

signal. In principle, ultrasound-modulated light can be measured within an ultrasound period, which is on the order of a microsecond. In practice, the speckle decorrelation time that can be handled by FLUX is likely to be limited by the sampling time window, within which sufficient photons should be detected to achieve a high enough signal-to-noise ratio (SNR). In comparison, optical-wavefront-shaping-based approaches (the most competitive alternative methods) require the sample to be stable during the entire cycle of operation, including signal measurement, transfer, processing and wavefront modulation, which fundamentally prevents these approaches from working with highly dynamic scattering media. A detailed comparison of these two techniques is illustrated in Supplementary Fig. 1 to explain the advantage of FLUX in the presence of fast speckle decorrelation.

Generalized FLUX model. Here, we develop a generalized mathematical framework for FLUX, where we no longer assume the fluorescent object and the ultrasound focus are of the same size. We impose a grid on the sample with a voxel size equal to the speckle grain size; this grid covers the entire illumination volume. The fluorophores are dispersed in the sample with a distribution described by the number of fluorophores N_i in a voxel, where i denotes the i th voxel. For simplicity, we assume each voxel is illuminated by a fully developed time-varying speckle with intensity $I(t)$, which has a mean of I_0 , a variance of I_0^2 and a decorrelation time of τ_d . The ultrasound focal volume is V and covers M_{in} voxels.

The detected fluorescence photon count rate (proportional to intensity) is denoted as $F(t) = F_{ac}(t) + F_{dc}(t)$, where we separate out the time-varying and constant components. Similarly, the detected ultrasound-modulated photon count rate is denoted as $U(t) = U_{ac}(t) + U_{dc}(t)$. See Supplementary Note 1 for more details. We express the FLUX signal as:

$$FLUX = T \int_0^T F_{ac}(t) U_{ac}(t) dt, \tag{1}$$

where T is the total measurement time. The expectation of $FLUX$ is:

$$\begin{aligned} \langle FLUX \rangle &= T \int_0^T \langle F_{ac}(t) U_{ac}(t) \rangle dt \\ &= (I_0 q_f N_{in} T) (I_0 q_u V I_U T) \times \frac{1}{M_{in}}. \end{aligned} \tag{2}$$

The final expression relates $FLUX$ to experimental parameters. I_U is the ultrasound intensity, q_f and q_u are constants containing illumination-photon-to-signal-photon conversion efficiencies and detection efficiencies, and N_{in} is the fluorophore count within the ultrasound focus.

Notably, $FLUX$ is proportional to N_{in} and independent of the fluorophore count outside the ultrasound focus— $FLUX$ can therefore serve as a direct measure of the fluorophore count inside the ultrasound focus. $FLUX$ is inversely proportional to M_{in} . However, a full evaluation of the impact of M_{in} on the SNR of $FLUX$ measurement needs to account for its impact on the variance of $FLUX$ as well (see Supplementary Note 1 for an SNR analysis).

We can normalize the $FLUX$ signal to arrive at a dimensionless quantity

$$FLUX_{norm} = \frac{FLUX}{\sqrt{\langle \int_0^T |F_{ac}(t)|^2 dt \rangle \langle \int_0^T |U_{ac}(t)|^2 dt \rangle}}.$$

$FLUX_{norm}$ can be interpreted as a proportionate measure of the fluorophore fraction within the ultrasound focus, and it generally ranges from 0 to 1. It can also be interpreted as the correlation coefficient of $F(t)$ and $U(t)$.

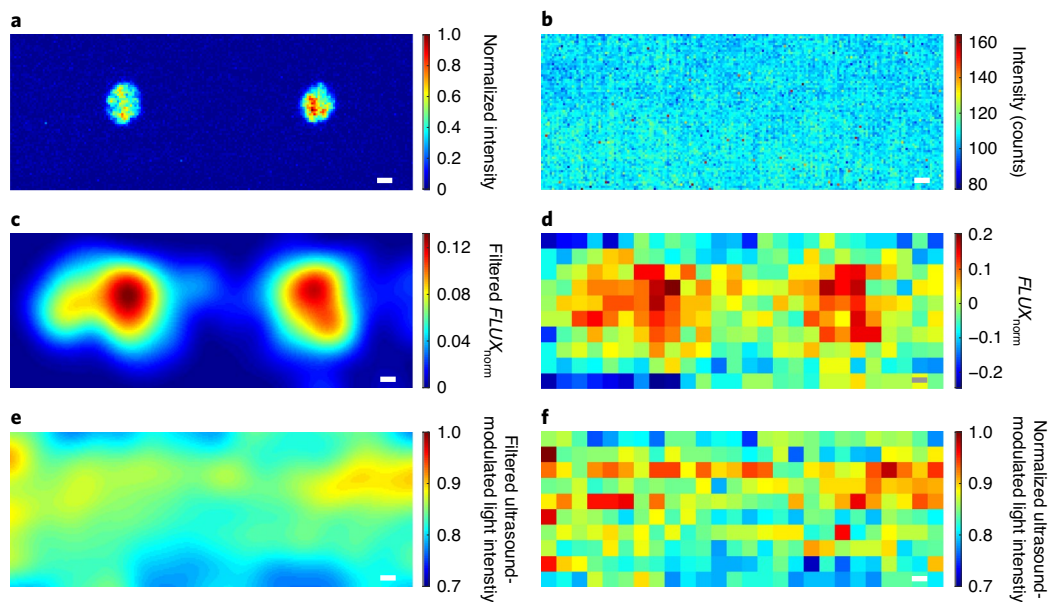


Fig. 3 | Imaging multiple fluorescent targets inside a dynamic scattering sample with a speckle decorrelation time of 17 ms. **a**, Direct wide-field image of the fluorescent targets, without the presence of any scattering media. **b**, Direct wide-field image when the fluorescent targets are sandwiched between two scattering diffusers. **c**, FLUX reconstructed image of the fluorescent targets between the scattering diffusers. **d**, Raw pixels of **c**; map of $FLUX_{norm}$ measured at each ultrasound focus position. **e**, Reconstructed image using the ultrasound-modulated light signal alone. **f**, Raw pixels of **e**; normalized ultrasound-modulated light signal measured at each ultrasound focus position. Scale bars, 10 μm .

The system point-spread-function is given by cross-correlating the speckle autocorrelation function with the ultrasound focal profile. When the optical speckle size is much smaller than the ultrasound focal size, the imaging resolution is defined by the ultrasound focal profile.

Imaging fluorescent targets within a dynamic scattering medium.

We built a proof-of-concept system to demonstrate the FLUX method. A fluorescent particle (10 μm in diameter) was sandwiched between two moving scattering diffusers (see Fig. 2a and Supplementary Fig. 2 for details). This configuration allows us to freely change the illumination speckle grain size and the speckle decorrelation time. We adjusted the diffusers to provide a mean speckle grain size of 39 μm at the fluorescent particle. Because the full-width at half-maximum (FWHM) of the lateral profile of the ultrasound focus is 38.8 μm , we have M_m nominally equal to one in this case. We adjusted the movement speeds of the diffusers to provide speckles with a decorrelation time of 17 ms on the camera (Fig. 2b). A single-photon-counting module was used to measure the fluorescence emission over time. Meanwhile, a focused single-cycle ultrasound pulse (50 MHz central frequency) was used to modulate light at a target location in the sample. The ultrasound-modulated light was measured with a lock-in parallel speckle measurement method⁴⁸ using a camera running at 1,123 frames per second (see Methods). Since we employed a dual-frame lock-in method, the effective sampling period of the ultrasound-modulated light was 1.8 ms.

The ultrasound focus was raster scanned over an area covering the fluorescent particle (on the x - y plane in Fig. 2a) with a step size of 10 μm . At each location, we collected $F(t)$ and $U(t)$ traces over a duration T of 4.5 s, and calculated $FLUX_{norm}$. An image of the fluorescent particle was then obtained by plotting $FLUX_{norm}$ as a function of ultrasound focus position and applying a bicubic interpolation to remove the pixelation effect (Fig. 2c). By fitting the experimental data with Gaussian functions, we find that the FWHM resolution is 74.8 μm along the x direction and 76.0 μm along the y direction, which matches reasonably with our

theoretical predictions of 61.2 μm (see Supplementary Fig. 3 for a detailed comparison).

Figure 2d shows examples of the time-varying fluorescence and ultrasound-modulated light signals measured at two ultrasound focus positions (x_1, y_1) and (x_2, y_2) denoted in Fig. 2c. The time-varying profiles of these signals are due to the motion of the front diffuser. When the ultrasound focus overlapped with the fluorescent object, we observed a high correlation between the fluorescence and ultrasound-modulated light signals ($FLUX_{norm} = 0.61$). In contrast, when the ultrasound focus was 64 μm away from the object, a low correlation was observed as expected ($FLUX_{norm} = 0.01$). The lower-than-expected measured maximum $FLUX_{norm}$ of 0.61 (in theory should be 1.0) is possibly attributed to the fluorescent particle itself deflecting some of the ultrasound-modulated light away from the detection solid angle. In this case, the weight of the ultrasound-modulated light outside the nominal ultrasound focal spot (FWHM of the ultrasound focal profile) increases. Therefore, there is effectively more than one speckle within the ultrasound focus.

In our control experiment, we attempted to directly image the fluorescent particle by focusing a camera at the plane of the particle through the diffusers. The direct fluorescence image is shown in Fig. 2e and Supplementary Fig. 4. We measured the fluorescent particle's lateral FWHM profile to be 1.3 mm—at least an order of magnitude poorer than our observed FLUX resolution.

We further profiled the performance of this system as a function of speckle decorrelation time. We parked the ultrasound focus at the particle and gradually changed the speckle decorrelation time. The measured $FLUX_{norm}$ as a function of speckle decorrelation time is shown in Fig. 2f. The measured $FLUX_{norm}$ decreased as the speckle decorrelation time was shortened. Nevertheless, our experiment showed that our proof-of-concept set-up can tolerate fast speckle decorrelation down to a speckle decorrelation time of 8 ms (when $FLUX_{norm}$ reduces to half of its plateaued value).

While the above experiment illustrates some key aspects of the FLUX approach, it is likely that in many applications, the illumination

speckle grains would be much smaller than the ultrasound focus. This leads to a high M_{in} value and subsequently to a reduced FLUX signal. Our next experiment aimed to examine the impact.

In this experiment, we adjusted the diffusers to generate illumination speckles of size $2.8\mu\text{m}$. The ultrasound FWHM focal spot size was kept at $38.8\mu\text{m}$, which gives a M_{in} value of 192. The fluorescent object consisted of two fluorescent beads of $\sim 30\mu\text{m}$ diameter and with $\sim 127\mu\text{m}$ separation. Figure 3a shows a direct wide-field image of the two fluorescent beads acquired by a conventional fluorescence imaging system. When the fluorescent beads were sandwiched between the scattering diffusers, they could not be resolved (Fig. 3b). To image through the scattering media using FLUX, we raster scanned the ultrasound focus with a step size of $10\mu\text{m}$ and reconstructed the image of the fluorescent object as shown in Fig. 3c. Figure 3d shows the raw map of $FLUX_{norm}$ at each ultrasound focus position. Two physical priors were imposed in the image processing (from Fig. 3d to Fig. 3c). First, the negative values of $FLUX_{norm}$ are due to noise and thus were set to zeros. Second, the image resolution is determined by the ultrasound focal size and therefore we applied a low-pass filter to filter out the frequency components that were higher than the ultrasound resolution. Finally, we applied interpolation to alleviate the pixelation effect. As a control experiment, Figs. 3e and 3f (Fig. 3e is the low-pass-filtered and interpolated version of Fig. 3f) show the map of ultrasound-modulated light signal at each ultrasound focus position, verifying that ultrasound-modulated light alone is not capable of imaging the fluorescent object.

This experiment shows that a speckle size of micrometre scale and a high M_{in} also allows FLUX to image through dynamic scattering samples. To assess FLUX's applicability to any scenario, we need to assess whether FLUX can be reliably and accurately measured. Put in mathematical terms, we require the SNR of FLUX, which equals FLUX mean divided by its standard deviation, to be substantially larger than unity in order for FLUX to function well. We report a detailed analysis in Supplementary Notes 1–3. Our experiment operates in a regime where the numbers of detected fluorescence and ultrasound-modulated light photons originating from a single illumination speckle grain per decorrelation time are much larger than unity, and hence the FLUX variance term associated with a finite measurement time (that is, speckle statistical noise) dominates over other noise sources (see Supplementary equations (9) and (10.1)). In this case, the SNR_{FLUX} equation can be derived by simplifying Supplementary equation (10). It takes the form

$$SNR_{FLUX} = \sqrt{\frac{T}{\tau_d}} \sqrt{\frac{M_{all} N_{in}}{M_{in} N_{all}}} \frac{1}{\sqrt{\gamma}},$$

where M_{all} is the number of fluorophore-bearing speckles in the whole sample, N_{in}/N_{all} is the fractional proportion of fluorophores in the ultrasound focus, and γ is a dimensionless quantity that is approximately equal to one and it takes into account the impact of fluctuating frequency content on the FLUX signal (see Supplementary Note 1). Using this equation, the theoretical SNR for our experiment is 17. In Supplementary Note 3, we provide an example calculation of the SNR for a practical imaging scenario in biological tissue.

Discussion

We have developed a method that enables imaging of fluorescent objects within highly dynamic scattering media. FLUX combines the advantages of light and sound synergistically—it allows us to image fluorescence contrast at the ultrasound resolution in turbid media. Intriguingly, the dynamic nature of such media has been a major confounding factor in wavefront-shaping-based methods. In contrast, this feature is no longer a problem but instead a key enabling factor of our method. In addition, FLUX does not require a phase conjugation module or any wavefront shaping set-up, substantially simplifying the hardware system.

In our experiments, the number of data points is on the order of 10^3 to 10^4 , which leads to a measurement time of 1 to 10 s for each image pixel. Therefore, FLUX is not a high-speed imaging method and is not suitable for imaging fluorophores that have a large displacement (that is, displacements larger than the ultrasound focal size) within a few seconds. It aims to overcome the fast speckle decorrelation (mainly caused by light scattered by flowing red blood cells in blood vessels) that poses a grand challenge for wavefront shaping techniques^{7–29} to achieve a focus in living tissue. In a properly immobilized sample, a fluorescent target is less likely to move more than the size of an ultrasound focus, that is, $\sim 50\mu\text{m}$, within a few seconds.

The performance of FLUX is related to the number of speckles in the ultrasound focus and in the fluorescent targets, the ratio of the total measurement time to the decorrelation time, the shot noise and the speckle statistical noise. The exact SNR expression is shown in Supplementary equation (10) and it provides a recipe for the analysis of potential FLUX application scenarios for feasibility. While the resolution of FLUX is primarily determined by the ultrasound focal size, methods such as high-order moment analysis^{31–33,49,50} can potentially be employed to improve the resolution.

One practical consideration worth analysing is the impact of a finite etendue of the ultrasound-modulated photon detection system, which adds undesirable fluctuations to the signal. When the ratio of the number of speckles within the ultrasound focus to the number of detected speckles is small, the impact of the finite etendue on the SNR of FLUX is small (see Supplementary Note 2).

In Supplementary Note 3, we examine the practical application of FLUX in biophotonics by considering the feasibility of imaging a fluorescent object located 3 mm deep in tissue. The analysis reveals that FLUX can potentially work well in providing ultrasound resolution imaging or long-timeline functional monitoring of a fluorescent target, provided that the background fluorophore count is not excessively high. Interestingly, the analysis also points out that the SNR is positively correlated with the ratio of the total measurement time to the speckle decorrelation time. As such, FLUX may work better if the sample is additionally perturbed to reduce the decorrelation time, provided that the FLUX variance term associated with shot noise is not dominant. The decorrelation time can also be reduced by using a well-conditioned fluctuating illumination light field. Other directions to improve the system are discussed in Supplementary Note 4.

Online content

Any methods, additional references, Nature Research reporting summaries, source data, extended data, supplementary information, acknowledgements, peer review information; details of author contributions and competing interests; and statements of data and code availability are available at <https://doi.org/10.1038/s41566-020-0630-0>.

Received: 28 January 2020; Accepted: 30 March 2020;
Published online: 11 May 2020

References

- Ntziachristos, V. Going deeper than microscopy: the optical imaging frontier in biology. *Nat. Methods* **7**, 603–614 (2010).
- Bertolotti, J. et al. Non-invasive imaging through opaque scattering layers. *Nature* **491**, 232–234 (2012).
- Katz, O., Heidmann, P., Fink, M. & Gigan, S. Non-invasive single-shot imaging through scattering layers and around corners via speckle correlations. *Nat. Photon.* **8**, 784–790 (2014).
- Katz, O., Small, E. & Silberberg, Y. Looking around corners and through thin turbid layers in real time with scattered incoherent light. *Nat. Photon.* **6**, 549–553 (2012).
- Papadopoulos, I. N., Jouhannau, J. S., Poulet, J. F. A. & Judkewitz, B. Scattering compensation by focus scanning holographic aberration probing (F-SHARP). *Nat. Photon.* **11**, 116–123 (2017).

6. Yoon, S. et al. Deep optical imaging within complex scattering media. *Nat. Rev. Phys.* **2**, 141–158 (2020).
7. Yaqoob, Z., Psaltis, D., Feld, M. S. & Yang, C. Optical phase conjugation for turbidity suppression in biological samples. *Nat. Photon.* **2**, 110–115 (2008).
8. Popoff, S. M. et al. Measuring the transmission matrix in optics: an approach to the study and control of light propagation in disordered media. *Phys. Rev. Lett.* **104**, 100601 (2010).
9. Mosk, A. P., Lagendijk, A., Lerosey, G. & Fink, M. Controlling waves in space and time for imaging and focusing in complex media. *Nat. Photon.* **6**, 283–292 (2012).
10. Vellekoop, I. M. & Mosk, A. P. Focusing coherent light through opaque strongly scattering media. *Opt. Lett.* **32**, 2309–2311 (2007).
11. Rotter, S. & Gigan, S. Light fields in complex media: mesoscopic scattering meets wave control. *Rev. Mod. Phys.* **89**, 015005 (2017).
12. Yu, H. et al. Recent advances in wavefront shaping techniques for biomedical applications. *Curr. Appl. Phys.* **15**, 632–641 (2015).
13. Park, J. H., Yu, Z., Lee, K. R., Lai, P. & Park, Y. K. Perspective: wavefront shaping techniques for controlling multiple light scattering in biological tissues: toward in vivo applications. *APL Photon.* **3**, 100901 (2018).
14. Jang, M. et al. Relation between speckle decorrelation and optical phase conjugation (OPC)-based turbidity suppression through dynamic scattering media: a study on in vivo mouse skin. *Biomed. Opt. Express* **6**, 72–85 (2015).
15. Qureshi, M. M. et al. In vivo study of optical speckle decorrelation time across depths in the mouse brain. *Biomed. Opt. Express* **8**, 4855–4864 (2017).
16. Liu, Y. et al. Optical focusing deep inside dynamic scattering media with near-infrared time-reversed ultrasonically encoded (TRUE) light. *Nat. Commun.* **6**, 5904 (2015).
17. Akbulut, D., Huisman, T. J., van Putten, E. G., Vos, W. L. & Mosk, A. P. Focusing light through random photonic media by binary amplitude modulation. *Opt. Express* **19**, 4017–4029 (2011).
18. Cui, M. A high speed wavefront determination method based on spatial frequency modulations for focusing light through random scattering media. *Opt. Express* **19**, 2989–2995 (2011).
19. Wang, D. et al. Focusing through dynamic tissue with millisecond digital optical phase conjugation. *Optica* **2**, 728–735 (2015).
20. Conkey, D. B., Caravaca-Aguirre, A. M. & Piestun, R. High-speed scattering medium characterization with application to focusing light through turbid media. *Opt. Express* **20**, 1733–1740 (2012).
21. Stockbridge, C. et al. Focusing through dynamic scattering media. *Opt. Express* **20**, 15086–15092 (2012).
22. Kim, D. et al. Toward a miniature endomicroscope: pixelation-free and diffraction-limited imaging through a fiber bundle. *Opt. Lett.* **39**, 1921–1924 (2014).
23. Ma, C., Zhou, F., Liu, Y. & Wang, L. V. Single-exposure optical focusing inside scattering media using binarized time-reversed adapted perturbation. *Optica* **2**, 869–876 (2015).
24. Liu, Y., Ma, C., Shen, Y. & Wang, L. V. Bit-efficient, sub-millisecond wavefront measurement using a lock-in camera for time-reversal based optical focusing inside scattering media. *Opt. Lett.* **41**, 1321–1324 (2016).
25. Blochet, B., Bourdieu, L. & Gigan, S. Focusing light through dynamical samples using fast continuous wavefront optimization. *Opt. Lett.* **42**, 4994–4997 (2017).
26. Liu, Y., Ma, C., Shen, Y., Shi, J. & Wang, L. V. Focusing light inside dynamic scattering media with millisecond digital optical phase conjugation. *Optica* **4**, 280–288 (2017).
27. Tzang, O. et al. Wavefront shaping in complex media with a 350 kHz modulator via a 1D-to-2D transform. *Nat. Photon.* **13**, 788–793 (2019).
28. Xia, M., Li, D., Wang, L. & Wang, D. Fast optical wavefront engineering for controlling light propagation in dynamic turbid media. *J. Innov. Opt. Health Sci.* **12**, 1930007 (2019).
29. Wei, X. et al. Real-time frequency-encoded spatiotemporal focusing through scattering media using a programmable 2D ultrafine optical frequency comb. *Sci. Adv.* **6**, eaay1192 (2020).
30. Wang, L. V. & Hu, S. Photoacoustic tomography: in vivo imaging from organelles to organs. *Science* **335**, 1458–1462 (2012).
31. Gateau, J., Chaigne, T., Katz, O., Gigan, S. & Bossy, E. Improving visibility in photoacoustic imaging using dynamic speckle illumination. *Opt. Lett.* **38**, 5188–5191 (2013).
32. Chaigne, T. et al. Super-resolution photoacoustic fluctuation imaging with multiple speckle illumination. *Optica* **3**, 54–57 (2016).
33. Chaigne, T., Arnal, B., Vilov, S., Bossy, E. & Katz, O. Super-resolution photoacoustic imaging via flow-induced absorption fluctuations. *Optica* **4**, 1397–1404 (2017).
34. Lichtman, J. W. & Conchello, J.-A. Fluorescence microscopy. *Nat. Methods* **2**, 910–919 (2005).
35. Kobayashi, M., Mizumoto, T., Shibuya, Y., Enomoto, M. & Takeda, M. Fluorescence tomography in turbid media based on acousto-optic modulation imaging. *Appl. Phys. Lett.* **89**, 181102 (2006).
36. Huynh, N. T., Hayes-Gill, B. R., Zhang, F. & Morgan, S. P. Ultrasound modulated imaging of luminescence generated within a scattering medium. *J. Biomed. Opt.* **18**, 20505 (2013).
37. Liu, Y., Feshitan, J. A., Wei, M.-Y., Borden, M. A. & Yuan, B. Ultrasound-modulated fluorescence based on fluorescent microbubbles. *J. Biomed. Opt.* **19**, 85005 (2014).
38. Zhang, Q., Morgan, S. P. & Mather, M. L. Nanoscale ultrasound-switchable FRET-based liposomes for near-infrared fluorescence imaging in optically turbid media. *Small* **13**, 1602895 (2017).
39. Yuan, B., Uchiyama, S., Liu, Y., Nguyen, K. T. & Alexandrakis, G. High-resolution imaging in a deep turbid medium based on an ultrasound-switchable fluorescence technique. *Appl. Phys. Lett.* **101**, 033703 (2012).
40. Xu, X., Liu, H. & Wang, L. V. Time-reversed ultrasonically encoded optical focusing into scattering media. *Nat. Photon.* **5**, 154–157 (2011).
41. Wang, Y. M., Judkewitz, B., DiMarzio, C. A. & Yang, C. Deep-tissue focal fluorescence imaging with digitally time-reversed ultrasound-encoded light. *Nat. Commun.* **3**, 928 (2012).
42. Si, K., Fiolka, R. & Cui, M. Fluorescence imaging beyond the ballistic regime by ultrasound pulse guided digital phase conjugation. *Nat. Photon.* **6**, 657–661 (2012).
43. Horstmeyer, R., Ruan, H. & Yang, C. Guidestar-assisted wavefront-shaping methods for focusing light into biological tissue. *Nat. Photon.* **9**, 563–571 (2015).
44. Blochet, B., Joaquina, K., Blum, L., Bourdieu, L. & Gigan, S. Enhanced stability of the focus obtained by wavefront optimization in dynamical scattering media. *Optica* **6**, 1554–1561 (2019).
45. Resink, S. G., Boccara, A. C. & Steenbergen, W. State-of-the-art of acousto-optic sensing and imaging of turbid media. *J. Biomed. Opt.* **17**, 40901 (2012).
46. Elson, D. S., Li, R., Dunsby, C., Eckersley, R. & Tang, M.-X. Ultrasound-mediated optical tomography: a review of current methods. *Interface Focus* **1**, 632–648 (2011).
47. Gunther, J. & Andersson-Engels, S. Review of current methods of acousto-optical tomography for biomedical applications. *Front. Optoelectron.* **10**, 211–238 (2017).
48. Ruan, H., Mather, M. L. & Morgan, S. P. Pulsed ultrasound modulated optical tomography utilizing the harmonic response of lock-in detection. *Appl. Opt.* **52**, 4755–4762 (2013).
49. Dertinger, T., Colyera, R., Iyer, G., Weiss, S. & Enderlein, J. Fast, background-free, 3D super-resolution optical fluctuation imaging (SOFI). *Proc. Natl Acad. Sci. USA* **106**, 22287–22292 (2009).
50. Doktovsky, D., Rosenfeld, M. & Katz, O. Acousto optic imaging beyond the acoustic diffraction limit using speckle decorrelation. *Commun. Phys.* **3**, 5 (2020).

Publisher's note Springer Nature remains neutral with regard to jurisdictional claims in published maps and institutional affiliations.

© The Author(s), under exclusive licence to Springer Nature Limited 2020

Methods

System set-up. All data shown were recorded using a custom-built experimental set-up schematically shown in Supplementary Fig. 2a. To achieve a high spatial resolution along the acoustic axis for ultrasound-modulated light detection, a pulsed laser was used as the light source (Navigator, Spectra-Physics; 532-nm wavelength, 7-ns pulse width, externally triggered at 80 kHz). The laser beam passed through an isolator, a variable attenuator composed of a half-wave plate and a polarizing beamsplitter. To maximize the speckle contrast, the light was spatially filtered by a single-mode fibre and polarized after collimation.

The laser beam illuminated a scattering sample composed of two light-scattering diffusers D1 and D2 (DG10-120A, Thorlabs). (The diffuser does not transmit a detectable ballistic photon measured with a detection threshold of less than 1×10^{-5} of the transmitted power.) Fluorescent beads (FluoSpheres Polystyrene Microspheres, Life Technologies, 540/560 nm) were embedded as an imaging object in a 1.5% carrageenan gel and sandwiched between the two diffusers. The goal was to image the object through the scattering diffusers. To quantitatively induce speckle decorrelation, the two diffusers were translated by motorized stages along the x axis (Fig. 2a), and the speckle decorrelation time on the camera (shown in Fig. 1a) was tuned by controlling the movement speeds. The speeds of the diffusers were set so that the decorrelation times on the camera due to the motion of each diffuser are the same. We determined the decorrelation time by capturing a sequence of speckle patterns on the camera and computing the correlation coefficients of pairs of patterns with various time intervals^{16,19,26}. The decorrelation time is defined as the time interval during which the correlation coefficient reduces to 50% (Fig. 2b).

The emitted fluorescent light was collected by an objective lens (MY10X-803, Mitutoyo, 10 \times , 0.28 numerical aperture (NA)), reflected by a dichroic mirror (FF541-SDi01-25 \times 36, Semrock), filtered by a fluorescent filter (561-nm long pass and 550-nm long pass), focused by a lens (30-mm focal length) and detected by a single-photon-counting module (SPCM-AQRH-14, PerkinElmer). A multifunctional data acquisition board (PCIe-6363, National Instruments) was used to count the photons at the same time as the ultrasound-modulated light measurement.

A spherically focused ultrasound transducer (V3330, Olympus; 50-MHz central frequency) was driven by a power amplifier (30W1000B, Amplifier Research) and raster scanned on the object plane by a motorized stage (MP-285, Sutter Instruments). At each ultrasound focus position, pulsed ultrasound-modulated light was detected by using a lock-in parallel speckle measurement method based on a camera (see next section ‘Measurement of ultrasound-modulated pulsed light’ for more details), which achieved a large etendue⁴⁸. Before inserting the scattering diffusers, the object plane was virtually imaged to the camera through a 4f system composed of the objective lens and a tube lens. The duration for measuring the ultrasound-modulated light signal at each time point was 1.78 ms. The number of sampling points of the signal traces for reconstructing each pixel in Fig. 2c and Fig. 3d were 3,000 and 20,000, respectively.

Measurement of ultrasound-modulated pulsed light. We used a lock-in parallel speckle measurement method based on a camera (pco.edge 5.5, PCO-TECH; global shutter, 500- μ s exposure time, externally triggered, running at 1,123 frames per second with $64 \times 2,560$ pixels) to measure the ultrasound-modulated light in two frames. The signal to drive the ultrasound transducer was a single-cycle pulse train, and the pulses were inverted during the second frame (Supplementary Fig. 2b). This pulse inversion was achieved by using a switch (ZX80-DR230-S+, Mini-Circuits) to switch the signal between two pulse trains with inverted pulses

generated by two function generators (AFG 3252C, Tektronix). See Supplementary Fig. 2b for more details about the signal diagram.

Since the laser pulses were shorter than the ultrasound pulses, and they were synchronized, the interference patterns between the modulated light and unmodulated light were locked by the laser pulses and became static on the camera. Mathematically, the intensities on each pixel of the camera recorded in the two frames can be written as $I_1(\mathbf{r}) = I_M(\mathbf{r}) + I_U(\mathbf{r}) + 2\sqrt{I_M(\mathbf{r})I_U(\mathbf{r})}\cos[\varphi_M(\mathbf{r}) - \varphi_U(\mathbf{r})]$ and $I_2(\mathbf{r}) = I_M(\mathbf{r}) + I_U(\mathbf{r}) + 2\sqrt{I_M(\mathbf{r})I_U(\mathbf{r})}\cos[\varphi_M(\mathbf{r}) - \varphi_U(\mathbf{r}) + \pi]$, where r is the pixel centre location, I_M and I_U are the intensities of the ultrasound-modulated light and unmodulated light, and φ_M and φ_U are the phases of the ultrasound-modulated light and unmodulated light. By subtracting the two images, we obtain $\Delta I(\mathbf{r}) = 4\sqrt{I_M(\mathbf{r})I_U(\mathbf{r})}\cos[\varphi_M(\mathbf{r}) - \varphi_U(\mathbf{r})]$. Since I_M , I_U , φ_M and φ_U are independent, and φ_M and φ_U follow a uniform distribution between $[0, 2\pi)$ while I_M and I_U follow an exponential distribution, by squaring $\Delta I(\mathbf{r})$ and averaging over the speckle pattern, we have the equation $\langle [\Delta I(\mathbf{r})]^2 \rangle = 8\bar{I}_M\bar{I}_U$, where $\langle \cdot \rangle$ denotes ensemble averaging over the detected speckle pattern on the camera, and \bar{I}_M and \bar{I}_U are the mean intensities of the speckle patterns formed by the ultrasound-modulated and unmodulated light, respectively. Since \bar{I}_U can be approximated to a constant number over different realizations of speckle patterns, the quantity $\langle [\Delta I(\mathbf{r})]^2 \rangle$ is proportional to the power of the ultrasound-modulated light within the ultrasound focus and thus considered as the ultrasound-modulated light signal.

Data availability

The data that support the plots within this paper and other findings of this study are available from the corresponding authors upon reasonable request.

Code availability

The code that supports the plots within this paper and other findings of this study is available from the corresponding authors upon reasonable request.

Acknowledgements

This work was supported by the Kernel-Brain Research and Technologies fund (FS 13520230) and the Rosen Bioengineering Center Endowment Fund (9900050).

Author contributions

H.R. conceived the idea. H.R., Y.L. and C.Y. developed the idea and designed the experiments. Y.L. and H.R. developed the experimental protocol and set-up. Y.L. constructed the samples and conducted the imaging experiments. H.R. and Y.L. analysed the data. C.Y., J.X., H.R., Y.L. and Y.H. conducted the theoretical analysis. All authors contributed to the preparation of the manuscript.

Competing interests

The authors declare no competing interests.

Additional information

Supplementary information is available for this paper at <https://doi.org/10.1038/s41566-020-0630-0>.

Correspondence and requests for materials should be addressed to H.R., Y.L. or C.Y.

Reprints and permissions information is available at www.nature.com/reprints.